Designing asymmetrically modified nanochannel sensors using virtual EIS

Sivaranjani Devarakonda, Sungu Kim, Baskar Ganapathysubramanian*, Pranav Shrotriya*

Department of Mechanical Engineering, Iowa State University, Ames, IA

Abstract

Monitoring electrochemical impedance changes across an asymmetrically functionalized nanochannel array provides an attractive mechanism for chemical and biological sensors. Specific binding of the receptor molecules with their analyte leads to changes in charge distribution on the nanochannel surfaces modifying the ionic transport across them. The magnitude of impedance change due to receptor/ligand binding or sensor sensitivity depends on a large number of parameters and consequently, identification of parameters that result in sensitive and specific sensing performance is extremely tedious and cost-intensive. We rely on a 'virtual EIS' procedure that models the transient ionic current due to a step-change in voltage to determine the frequency-dependent impedance of an asymmetrically functionalized nanochannel. This procedure is used to predict the impedance changes due to the specific binding of thrombin on nanochannel surfaces. Surface charge changes associated with the binding of thrombin protein on the aptamer coated surface result

*Corresponding authors

Email addresses: baskarg@iastate.edu (Baskar Ganapathysubramanian), shrotriy@iastate.edu (Pranav Shrotriya)

in a decrease of the membrane impedance and computational results suggest that a reduction in the ionic strength of the electrolyte leads to an increase in the magnitude of binding induced impedance reduction. Sensing experiments with thrombin binding aptamer are performed to evaluate the trends from the high-throughput computations. The agreement between model predictions and experimental observations suggests that the present modeling approach may be utilized to computationally evaluate sensor performance for a range of parameters and rapidly identify sensor configurations that enable point-of-care diagnostic devices with improved sensitivities.
Keywords: Nanoporous alumina, surface charge, virtual electrochemical impedance spectroscopy (EIS), thrombin

1. Introduction

Nanochannels with large aspect ratios (radius to length ~ 1000) are being investigated for biomedical applications including sensing[1–3], sequencing[4–6], gating and drug delivery[7–10]. Sensors based on solid state nanopores and nanochannels[11–14] with either asymmetric geometry (rectangular, cylindrical, conical) or asymmetric surface functionalization have demonstrated highly sensitive and specific performance using the phenomenon of ionic current rectification[15–20]. However, large scale application of these sensors is limited as the fabrication of single nanopores requires sophisticated nanofabrication techniques with expensive equipment. Asymmetrically functionalized anodized aluminium oxide (AAO) membranes with arrays of nanochannels are easy to fabricate and functionalize[21], and thus provide an economic and accessible platform for sensitive detection of analytes.[22–26]

Receptor molecules such as antibodies or aptamers that have specific affinity towards the desired analyte can be immobilized on the AAO membranes for highly specific sensors. Aptamers are short chain oligonucleotides that are becoming an ideal option as they are robust, stable, cost-effective and offer great flexibility to be tailored suitably to achieve higher affinities[27,28]. The specific binding between the ligand and aptamer molecules immobilized on the nanochannel surface is associated with changes in molecular conformations and charge distributions. When the size of the target analyte/receptor complex is comparable to nanochannel dimensions, steric effects dominate causing decline in nanochannel conductivity upon interaction with the analyte[24,26,29,30]. Kant et al.[30] have developed an impedance based biosensor and studied the effect of nanopore geometry on sensitivity using biotin as the model analyte. They have shown that the sensitivity can be boosted by reducing pore dimensions. Hence, optimization of nanochannel dimensions and fabrication of nanochannels with smaller diameters is needed for steric hindrance mechanism based sensors.

Nanochannel biosensors that rely on detecting the receptor/analyte binding induced surface charge modulation provide additional advantages[31] and a prospect for tuning sensitivities by altering parameters such as electrolyte concentration, nanochannel geometry and receptor density. Wang et al.[32] carried out a charge-based detection of DNA-DNA interactions in nanochannels using conductance as signal and they could achieve high sensitivity even with nanochannels with larger diameters at low electrolyte concentrations. Vlassiouk et al.[31] developed a nanofluidic diode biosensor using single conical nanopores with asymmetric charge distribution. The influence of surface

charges and geometry on ionic transport across charged nanochannels can be modeled numerically and utilized for optimizing sensor response[33–36]. Daiguji et al.[35] studied the effect of modifying surface charge on ionic transport through high aspect ratio nanochannels with overlapping ionic double layers. Ma et al.[37] studied entrance charge effects on ionic conductance using three charge configurations of nanochannels for building sensitive nanofluidic biosensors.

Previous modeling studies have relied on steady state solutions of ion-transport to estimate the changes in rectification factor or conductance due to surface charge changes. The electrical double layer formation inside the nanochannels is a transient phenomenon and recent experimental results show that frequency dependent transmembrane impedance may provide an efficient mechanism for specific sensing of ligands in presence of large concentrations of interfering molecules[23,38]. Modeling the transient or frequency dependent ionic conduction in the nanochannels will enable identification of performance parameters that enhance the sensor sensitivity and specificity.

We report a computational approach that serves as a virtual electrochemical impedance spectroscopy (EIS) to determine the impedance of asymmetrically functionalized nanochannel. We utilize the numerical results to identify the processing parameters that enhance sensitivity for Thrombin protein sensing using thrombin binding aptamer (TBA). Thrombin binding aptamer (TBA), a 15mer (GGTTGGTGTGGTTGG) binds to human α-thrombin reversibly via electrostatic interactions[39,40]. Binding reaction between protein and TBA involves interaction of the positively charge moieties on the protein to the TT loops and TGT loop on the aptamer, respec-

tively[41–43] and quenching of the negative charge of the aptamer. Electrochemical impedance spectroscopy (EIS) is used to monitor the impedance changes in asymmetric functionalized nanochannels using a four-electrode setup. The nanochannel arrays are asymmetrically functionalized through deposition of thin gold film on the nanochannel opening and modifying the gold-coated region with a thiol terminated TBA. Experimental measurements of the impedance changes on aptamer/thrombin binding are compared with numerical predictions to demonstrate the efficacy of virtual EIS identifying processing parameters that enhance sensor sensitivity.

2. Materials and Methods

2.1. Theoretical model

The electric current is modeled by the Nernst-Planck equation, which describes charged species transport in electrolyte in terms of convection, diffusion, and electric migration:

$$\vec{j}_i = \vec{u}c_i - \nabla c_i - D_i \frac{z_i F}{RT} c_i \nabla \phi, \tag{1}$$

where $\vec{j}$, $\vec{u}$, c_i, and ϕ are flux of species i, fluid velocity, species concentration, and potential. D_i is the diffusion coefficient, z_i is charge valence, F is Faraday number, R is gas constant, and T is temperature. The fluid resistance is high at the nanochannel; therefore, the convection is neglected in this study. The temporal variations of the species concentration can be evaluated by considering mass conservation:

$$\frac{dc_i}{dt} - \nabla \cdot (\nabla c_i + D_i \frac{z_i F}{RT} c_i \nabla \phi) = 0. \tag{2}$$

The chemical reactions at the electrodes are neglected. To close the equation (eq 2), we introduce Poisson equation,

$$-\varepsilon_0 \varepsilon_r \nabla^2 \phi = \rho_e, \tag{3}$$

where ρ_e is local charge density,

$$\rho_e = F \sum_{i=1}^{N} z_i c_i. \tag{4}$$

ε_0 and ε_r are the absolute and relative permittivity. The validation of the computational code is shown in supplementary material.

Fig 1(B) shows the theoretical model of a single nanochannel employed with asymmetric charge distribution. To minimize the computational cost, we focus on a single nanochannel (with length, 1 µm, and width, 20 nm) which can be easily extended to an array of nanochannels. For the boundary conditions, the species concentration is held equal to bulk electrolyte at both inlet and outlet reservoir (the left and right ends in Fig 1(B)). The study was performed employing NaCl as the electrolyte and the effect of electrolyte strength on sensitivity was studied by incorporating a hundred-fold dilution in our model. No-flux condition was assumed on all the other boundaries. The potential was controlled at both ends, V_{app}, 5mV on the left end and ground on the right end. The surface charge for aptamer modified region, σ_{DNA} was applied to a depth of 250 nm (h_{DNA}) assuming that the sputter-coated gold has penetrated to a reasonable extent into the nanochannels. For the rest of the nanochannel, a positive surface charge, σ_{AAO} was applied. Assuming the channel wall is insulating, the surface charge density is transformed in to Neumann boundary conditions[44].

$$\nabla \phi \cdot \vec{n} = -\frac{\sigma_{DNA/AAO}}{\epsilon_0 \epsilon_r}. \tag{5}$$

$\vec{n}$ is surface normal vector. There is no electric field across all the other boundaries,

$$\nabla\phi \cdot \vec{n} = 0. \tag{6}$$

2.2. Materials

The AAO membrane (Sigma Aldrich, Whatman), having nominal nanochannel diameters of 20 nm and membrane thickness of 50 μm, were used for the experiments. Thiol-modified thrombin-binding aptamer (TBA) was obtained from Integrated DNA Technologies (IDT) with the sequence 5'-/ThioMC6-D/GCCTTAACTGTAGTACTGGTGAAATTGCTGCCATT**GGTTGGTG TGGTTGG**-3'. The bolded portion of the sequence denotes the aptamer sequence that binds selectively to human α-thrombin. Human α-thrombin and mercapto-1-hexanol (MCH) were procured from Thermo-Fisher Scientific. Sensing experiments were performed in a buffer solution: 137 mM NaCl, 2.7 mM KCl, 10 mM Na_2HPO_4, 2 mM KH_2PO_4, pH 7.4 at room temperature. All the chemicals used for electrolyte were purchased from Sigma-Aldrich. All solutions were prepared with distilled deionized water (ddH_2O) produced by a Corning Mega-Pure system.

2.3. Membrane preparation

The AAO membranes were cleaned/sonicated with isopropanol, ethanol and ddH_2O. Then, one side of the membranes was sputter-coated with gold ($\sim$ 50 nm thickness), followed by washing again with isopropanol, ethanol and ddH_2O. Thiolated-TBA received from IDT was stored at higher concentration of 100 µM at -20°C. Before an experiment, aliquots of 1 µM TBA were prepared in the buffer and were heated to 95°C, 5 mM of $MgCl_2$ was

added and the solution was cooled down to room temperature (RT) slowly over a period of at least 45 min. Then the gold coated AAO membranes were incubated in the TBA solution at RT for 12 h to immobilize the TBA. The AAO membrane was then washed with the buffer containing 5 mM $MgCl_2$ and further incubated for 1 h at room temperature in 3 mM MCH (in ddH_2O) to block the gold surface not covered with TBA followed by washing with the buffer again.

2.4. EIS measurement

The four-electrode method was utilized to measure the impedance changes across the AAO membrane and nanochannel resistance extracted by fitting the EIS data to a circuit consisting of two Randles circuits in series. Platinum wires were used as the working (WE) and counter electrodes (CE) while Ag/AgCl wires were used as the two reference electrodes (RE). EIS was carried out with an AC perturbation signal of 5 mV, within the frequency range of 100 kHz-0.1 Hz. Fig 1(A) illustrates EIS measurement with four electrode setup. For all electrochemical experiments a custom-made Teflon cell (Fig 1(C)) was used. Equal volumes of protein solution (α-thrombin as analyte and γ-thrombin as negative control) prepared in the buffer were injected onto the port of the Teflon cell containing the TBA functionalized side of the membrane. The concentration of each injection was determined to achieve the desired target concentration inside the electrochemical cell to obtain a calibration curve for the experiment. In experiments done to study the effect of electrolyte ionic strength on sensitivity, the electrolyte and the protein dilutions were done in the buffer diluted by 100-fold. For all cases, the system was tested separately for selectivity using γ-thrombin as negative

control.

3. Results and Discussion

3.1. Virtual EIS based parametric exploration

Finite element-based solution of the Poisson-Nernst-Plank equations[45] is used to model the transient ionic current due to a step voltage change in the nanochannel with charged surfaces as shown in Fig 1. Fast Fourier transform of the derivative of the current response is used to determine the magnitude and phase of the frequency dependent impedance on the nanochannels. This approach is well developed for use in experimental investigations[46–49] and has been applied in the present work as a suitable method for computational determination of EIS spectrum. Fig 2(A) shows the typical current response and derivative of the current response for an applied step voltage of 5 mV. An initial spike as high as 1.2×10^6 A/(m.s) can be seen from the derivative of the current plot indicating the initial response of the system to step input. Bode and Nyquist plots for the computed impedance are plotted in Figs 2(B) and (C), respectively. Both Bode and Nyquist plots obtained numerically are similar to the plots obtained from electrochemical impedance spectroscopy of asymmetrically functionalized nanoporous membranes.

The sensor response of membrane depends on a number of different parameters including electrolyte concentration, nanochannel diameter, aspect ratio, and functionalization, among other variables. Experimental investigations to characterize the influence of each parameter on the sensor response can become resource expensive and time consuming. Hence, numerical investigations are a promising approach to quantify the influence of the parameters

and identify the sensing conditions that maximize the sensor response. We numerically investigated the effect of electrolyte ionic strength on the sensitivity of nanochannel impedance. Impedance of the nanochannels were predicted for high electrolyte concentrations (100 mM) as well as low electrolyte concentrations (1 mM). Front surface and quarter depth of the nanochannel are functionalized with negative surface charges, while the rest of the nanochannel depth and back surface are covered with positive surface charge (Fig 1). The asymmetric charge distribution models the aptamer functionalization of membranes used for biosensors[23]. In experiments, one of the membrane surfaces and a portion of its depth are coated with gold and a monolayer of aptamers is immobilized on the gold coated surface. Meanwhile, the back surface and remaining depth of the alumina film are left uncoated. The surface functionalized with nucleic acid aptamers monolayer is negatively charged while the uncoated surface is covered with low positive surface charge density accounting for protonated -OH groups at pH 7.4[50].

Surface charge density of the functionalized aptamer monolayer is based on a sequence length of 50 nucleotides and typical grafting density of 10^{12} chains/cm^2[51]. Accounting for Manning condensation[52], the DNA surface charge density is computed as:

$$\sigma_{DNA} = e\delta N f \tag{7}$$

where, e is the electron charge, N is the number of bases, δ is grafting density. The charging fraction, f, is given by, $f = b/l_B$, where b the separation per charge, l_B is the Bjerrum length defined as $l_B = e^2/\epsilon k_B T$, ϵ is relative permittivity of the medium, k_B the Boltzmann constant and T is the temperature. For most polyelectrolytes, b is equal to 0.4 nm and l_B is equal to 0.7 nm for

water and the magnitude of σ_{DNA} is computed to be -50 mC/m^2. Surface charge in the remaining non-functionalized portion of the nanochannel σ_{AAO} was assumed to be a low positive charge of 1 mC/m^2 [53,54]. The DNA/ligand binding is expected to quench the surface charges in the monolayer covering the nanochannel surface. The $\sigma_{DNA/ligand}$ is computed as:

$$\sigma_{DNA/ligand} = (1 - q)\sigma_{DNA} \tag{2}$$

where, q, is the degree of quenching or quenching fraction used to model the influence of ligand binding induced changes in surface charge density.

3.2. Effect of quenching fraction on EIS.

Impedance response across the asymmetrically charged nanochannel for different charge distributions are plotted for two electrolyte concentrations. Figs 3(A) and (B) show the computed Bode and Nyquist plots for q varying from 0 (-50 mC/m^2) to 0.9 (-5 mC/m^2) respectively. Computed Bode and Nyquist plots for the charged membrane at low electrolyte concentrations are plotted in Figs 3(C) and (D), respectively over the same range of quenching fractions. At both 100 mM and 1 mM concentrations of NaCl, the increase in quenching of the surface charge leads to reduction in the predicted nanochannel impedance. Channel resistance (R) is extracted from the impedance plots and the reduction in the channel resistance changes, ΔR, is plotted as a function of q in Fig 4. At both electrolyte concentrations, the reduction in R showed a bilinear trend. At high electrolyte concentrations, R decreased linearly as q increased from $q = 0$ (-50mC/m^2) to $q = 0.4$ (-30mC/m^2) but minimal changes in impedance are observed on further increase from $q = 0.4$ (-30 mC/m^2) to $q = 0.9$ (-5 mC/m^2). In contrast, at

low electrolyte concentrations, the reduction in R is gradual in the initial range of $q = 0$(-50mC/m^2) to $q = 0.4$ (-30mC/m^2) and the rate of reduction increases as quenching fraction is further increased from $q = 0.4$ (-30 mC/m^2) to $q = 0.9$ (-5 mC/m^2).

These impedance changes indicate that aptamer/ligand binding induced surface charge quenching modifies the ionic transport in the nanochannel. Large magnitude of surface charge changes are expected only on the specific binding between the ligand and aptamer monolayer. Physisorption of other molecules or non-specific binding is not expected to modify the surface charge distribution. Hence, impedance change may be utilized to detect binding between the aptamer modified surface and its specifically binding ligand. The sensing mechanism is different from biosensors based on steric hindrance where the channel resistance increases with binding of analytes due to blockage of the nanochannels. This is in contrast to surface charge modulation based sensing mechanism, where the nanochannel impedance will decrease (increase) if the surface charge magnitude is decreased (increased) on specific binding.

The slope of R change at low electrolyte concentration is about 7500 times larger than that at high electrolyte for the quenching fraction from 0 (-50 mC/m^2) to 0.4 (-30 mC/m^2) and is about 4.5x10^5 times larger for the quenching fraction range of 0.6 (-20 mC/m^2) to 0.9 (-5 mC/m^2). At low electrolyte concentrations, the debye length or extent of ionic double layer becomes larger and for the nanochannel, the debye length can become comparable to the nanochannel diameter resulting in counterions enrichment. The counterion enrichment will be strongly dependent on the surface charge

distribution and consequently, charge modulation may result in significant changes in ionic conduction across the nanochannel. Computed anion concentrations (Cl^-) are plotted in Figs 5 (A) and (B), respectively for higher and lower bulk electrolyte concentrations for monolayer charge density of -50 mC/m^2. At high ionic concentrations, only a narrow region adjacent to the DNA monolayer covered channel wall is devoid of any anions however at lower ionic concentration, anions are depleted across the whole channel in the DNA monolayer covered portion. The cation concentration distribution (included in supplementary information) shows that Na^+ ions get concentrated in the negatively charged region of the nanochannel and their concentration is 85 times larger for lower bulk concentrations in comparison to higher electrolyte concentrations. The surface charge induced segregation of the cations and anions in the nanochannel resists the ionic transport across the channel and this resistance is highly pronounced at lower ionic concentrations. Quenching of surface charges reduces the segregation and thus reduces the resistance to ionic transport. These effects are more pronounced at lower ionic concentration as the double layer extends across the whole nanochannel.

Slope of the normalized R changes due to quenching represents the sensitivity of the nanochannel impedance to aptamer/ligand binding and is presented in Table 1. These results indicate that reducing the electrolyte concentration from 100 mM to 1 mM, will result in 4.5 times increase of sensitivity for the quenching fraction from 0 (-50 mC/m^2) to 0.4 (-30 mC/m^2) and of about 240 times for the quenching fraction range of 0.6 (-20 mC/m^2) to 0.9 (-5 mC/m^2). Horn et al[40] estimated the number of surface charges on human α-thrombin at pH 7.4 to be 7/molecule and assuming 100% binding

efficiency between TBA and thrombin, maximum quenching of DNA monolayer is about 0.22 - 0.24 (11-12 mC/m^2). Sensing experiments of thrombin with thrombin aptamer coated membranes are conducted to investigate the postulated surface-charge-based sensing mechanism and increase in sensitivity at lower ionic concentrations over the quenching fraction range of 0 (-50 mC/m^2) to 0.4 (-30 mC/m^2).

3.3. Experimental validation of observed trends.

Bode and Nyquist plots for the experimentally measured impedance of the aptamer covered membrane in presence of different concentrations of α-thrombin are plotted in Figs 6(A) and (B), respectively for high electrolyte concentration of 100 mM and in Figs 6(C) and (D), respectively for low electrolyte concentration of 1 mM . The plots for both electrolyte strengths show that the impedance decreases with increasing concentrations of α-thrombin which is comparable to the simulation predictions. The impedance was fit to a two-loop model consisting of two Randles circuits in series (Fig 6(A) inset). The first loop corresponds to the higher frequency data and the second loop is for the lower frequency region. We observed through multiple experiments done on our system[23] with/without protein that the change in impedance observed due to TBA-thrombin binding is mainly in the higher frequency region. The lower frequency loop parameters varied randomly, independent of binding and may depend on electrodes used for the impedance measurement.

Similar observation was made by Wang et al[32], where they reported change in impedance occuring at relatively higher frequencies of 3 kHz and 10 kHz across a morpholino modified membrane due to surface charge modulation upon binding with target DNA. This indicates a strong frequency

dependence for impedance changes due to surface charge modulation. The changes in ionic double layer determine the impedance changes and consequently, the phenomena is primarily present in the high frequency region. Hence, the membrane parameters for the first loop, R (Nanochannel resistance) and C (Nanochannel capacitance) were extracted as parameters of interest.

Measured changes in R are plotted as a function of protein concentration of protein for both higher and lower electrolyte concentrations in Fig 7(A). We observed that R decreased as the membrane was exposed to increased concentrations of α-thrombin and this decrease was significant as compared to changes in other membrane parameters. The decrease in R was not observed when the membranes were exposed to a non-specific protein (γ-thrombin) indicating that only specific binding results in sensor response (supplementary information).

The specific binding between TBA and α-thrombin is expected to quench the surface charge in the DNA-covered region of the membrane. This surface charge modulation is responsible for the decrease in R. The sensor response was fitted to Langmuir isotherm and the dissociation coefficient, K_D, for TBA/protein binding was estimated to be about 0.27 nM and 0.59 nM in higher and lower electrolyte concentrations, respectively. The estimated values are comparable to K_D for TBA-thrombin of about 3 nM reported in solution[55]. It has been reported previously that the α-thrombin-TBA complex height above surface is about 2 nm[56]. The complex height is significantly smaller than the nanochannel diameter and hence, steric hindrances due to binding of α-thrombin to TBA are expected to be negligible. The slope of

the resistance change as a function of thrombin concentration in the linear region are determined to be 40.7 and 13648.64 at electrolyte concentration of 100 mM and 1mM, respectively indicating an increase of 335 times.

The magnitude of resistance change observed for each membrane depend on experimental parameters like the nanochannel size distribution, gold film thickness and aptamer functionalization. We normalized the resistance changes with the initial resistance of the membrane to facilitate comparison across different experimental conditions. Slope of the normalized resistance changes with thrombin concentration are compared to the virtual EIS based prediction in Table 1, to determine the sensor sensitivity at higher and lower electrolyte concentration. We observed that the sensitivity considering $\Delta R/R$ in the linear range (below K_D), the sensor signal increased by 2 times (Fig 7(B)) in the lower concentration medium which is less than what we saw in the simulation.

The predictions of sensitivity is for a single nanochannel assuming the gold coating to penetrate to about 250 nm into the channel, but it was hard to control the gold film penetration during sputter coating of membranes. Therefore, only a qualitative comparison with experimental results could be achieved. The sensitivity with which α-thrombin binds its aptamer decreases as the pH of the environment is increased/decreased[57]. The pH of the electrolyte in our case was reduced from 7.4 to 6.9 by diluting it by 100 times and this might be a possible reason for the sensitivity to increase only by a factor of 2 times with decreased ionic strength in our experiments as opposed to the predicted 4.5 times increase in the theoretical model. The experimental conditions should be optimized further, and well-controlled fabrication methods

may achieve the theoretically predicted sensitivities. Additional experimental and theoretical studies are required to fully optimize such nanoporous sensing systems.

4. Conclusions

We report a "virtual" EIS based approach to determine the sensing response due to binding of specific receptor molecules on aptamer functionalized nanochannels. Computational results indicate that quenching of surface charges in an asymmetrically functionalized nanochannel increases the transient ionic conductivity and the magnitude of change in conductivity increases with decrease in electrolyte concentration. Sensing experiments conducted to detect binding of thrombin proteins on aptamer modified alumina membranes show that the specific binding leads to increase in the transient ionic conductivity. Experimental measurements also show that reducing the electrolyte concentration results in higher sensitivity for thrombin detection. The agreement between virtual EIS computations and experimental observations demonstrates that computation of the transient response can provide insight into the mechanism governing asymmetric nanochannels based sensors. The virtual EIS computations may be used to optimize the sensor performance and can be utilized to build highly sensitive biosensing devices.

Author Contributions

Sivaranjani Devarakonda: Conceptualization, Investigation, Formal analysis, Writing original draft

Sungu Kim: Resources, Reviewing-Editing

Baskar Ganapathysubramanian: Conceptualization, Resources, Reviewing and Editing, Supervision, Funding acquisition

Pranav Shrotriya: Conceptualization, Writing-Reviewing and Editing Supervision, Funding acquisition

Supporting Information Supplementary data associated with this article can be found online. Consists of three sections

1. Validation of computational code used for vitual EIS
2. Concentration distribution of counter-ions in the nanochannel
3. Sensitivity test of the biosensor with γ-thrombin

Acknowledgements

Research reported in this publication was partially supported by NIDDK institute of the National Institutes of Health (Award No.: 5R44DK098031). Computing support from TG-CTS110007 is acknowledged. Support from the ISU Plant Science Institute is acknowledged. Helpful suggestions and technical discussions on the aptamer sensing experiments with Prof. Marit Nilsen-Hamilton are gratefully acknowledged.

Conflict of Interest

The authors declare no conflict of interest.

References

[1] A. de la Escosura-Muñiz, W. Chunglok, W. Surareungchai, A. Merkoçi, Nanochannels for diagnostic of thrombin-related diseases in human blood, Biosens. Bioelectron. 40 (1) (2013) 24–31.

[2] S. Z. Oo, G. Silva, F. Carpignano, A. Noual, K. Pechstedt, L. Mateos, J. A. Grant-Jacob, B. Brocklesby, P. Horak, M. Charlton, S. A. Boden, T. Melvin, A nanoporous gold membrane for sensing applications, Sens Biosensing Res 7 (2016) 133–140.

[3] S. G. Lemay, Nanopore-based biosensors: the interface between ionics and electronics, ACS Nano 3 (4) (2009) 775–779.

[4] Y. Feng, Y. Zhang, C. Ying, D. Wang, C. Du, Nanopore-based fourth-generation DNA sequencing technology, Genomics Proteomics Bioinformatics 13 (1) (2015) 4–16.

[5] I. Vlassiouk, P. Takmakov, S. Smirnov, Sensing DNA hybridization via ionic conductance through a nanoporous electrode, Langmuir 21 (11) (2005) 4776–4778.

[6] S.-J. Li, J. Li, K. Wang, C. Wang, J.-J. Xu, H.-Y. Chen, X.-H. Xia, Q. Huo, A nanochannel array-based electrochemical device for quantitative label-free DNA analysis, ACS Nano 4 (11) (2010) 6417–6424.

[7] R. Duan, F. Xia, L. Jiang, Constructing tunable nanopores and their application in drug delivery, ACS Nano 7 (10) (2013) 8344–8349.

[8] Y. Jiang, N. Liu, W. Guo, F. Xia, L. Jiang, Highly-efficient gating of solid-state nanochannels by DNA supersandwich structure containing ATP aptamers: a nanofluidic IMPLICATION logic device, J. Am. Chem. Soc. 134 (37) (2012) 15395–15401.

[9] F. Xia, W. Guo, Y. Mao, X. Hou, J. Xue, H. Xia, L. Wang, Y. Song, H. Ji, Q. Ouyang, Y. Wang, L. Jiang, Gating of single synthetic

nanopores by proton-driven DNA molecular motors, J. Am. Chem. Soc. 130 (26) (2008) 8345–8350.

[10] X. Li, T. Zhai, P. Gao, H. Cheng, R. Hou, X. Lou, F. Xia, Role of outer surface probes for regulating ion gating of nanochannels, Nat. Commun. 9 (1) (2018) 40.

[11] C. Dekker, Solid-state nanopores, Nat. Nanotechnol. 2 (4) (2007) 209–215.

[12] V. Mussi, P. Fanzio, L. Repetto, G. Firpo, P. Scaruffi, S. Stigliani, G. P. Tonini, U. Valbusa, DNA-functionalized solid state nanopore for biosensing, Nanotechnology 21 (14) (2010) 145102.

[13] M. Ali, S. Nasir, W. Ensinger, Bioconjugation-induced ionic current rectification in aptamer-modified single cylindrical nanopores, Chem. Commun. 51 (16) (2015) 3454–3457.

[14] X. Lin, A. P. Ivanov, J. B. Edel, Selective single molecule nanopore sensing of proteins using DNA aptamer-functionalised gold nanoparticles, Chem. Sci. 8 (5) (2017) 3905–3912.

[15] L.-J. Cheng, L. J. Guo, Rectified ion transport through concentration gradient in homogeneous silica nanochannels, Nano Lett. 7 (10) (2007) 3165–3171.

[16] R. Karnik, C. Duan, K. Castelino, H. Daiguji, A. Majumdar, Rectification of ionic current in a nanofluidic diode, Nano Lett. 7 (3) (2007) 547–551.

[17] X. Wang, J. Xue, L. Wang, W. Guo, W. Zhang, Y. Wang, Q. Liu, H. Ji, Q. Ouyang, How the geometric configuration and the surface charge distribution influence the ionic current rectification in nanopores, J. Phys. D Appl. Phys. 40 (22) (2007) 7077.

[18] I. Vlassiouk, S. Smirnov, Z. Siwy, Ionic selectivity of single nanochannels, Nano Lett. 8 (7) (2008) 1978–1985.

[19] L. Rosentsvit, W. Wang, J. Schiffbauer, H.-C. Chang, G. Yossifon, Ion current rectification in funnel-shaped nanochannels: Hysteresis and inversion effects, J. Chem. Phys. 143 (22) (2015) 224706.

[20] C. Wei, A. J. Bard, S. W. Feldberg, Current rectification at quartz nanopipet electrodes, Anal. Chem. 69 (22) (1997) 4627–4633.

[21] W. Lee, S.-J. Park, Porous anodic aluminum oxide: anodization and templated synthesis of functional nanostructures, Chem. Rev. 114 (15) (2014) 7487–7556.

[22] S.-H. Yeom, O.-G. Kim, B.-H. Kang, K.-J. Kim, H. Yuan, D.-H. Kwon, H.-R. Kim, S.-W. Kang, Highly sensitive nano-porous lattice biosensor based on localized surface plasmon resonance and interference, Opt. Express 19 (23) (2011) 22882–22891.

[23] A. Gosai, B. S. Hau Yeah, M. Nilsen-Hamilton, P. Shrotriya, Label free thrombin detection in presence of high concentration of albumin using an aptamer-functionalized nanoporous membrane, Biosens. Bioelectron. 126 (2019) 88–95.

[24] J. Deng, C.-S. Toh, Impedimetric DNA biosensor based on a nanoporous alumina membrane for the detection of the specific oligonucleotide sequence of dengue virus, Sensors 13 (6) (2013) 7774–7785.

[25] W. Ye, Y. Xu, L. Zheng, Y. Zhang, M. Yang, P. Sun, A nanoporous alumina membrane based electrochemical biosensor for histamine determination with biofunctionalized magnetic nanoparticles concentration and signal amplification, Sensors 16 (10) (Oct. 2016).

[26] S.-J. Li, N. Xia, B.-Q. Yuan, W.-M. Du, Z.-F. Sun, B.-B. Zhou, A novel DNA sensor using a sandwich format by electrochemical measurement of marker ion fluxes across nanoporous alumina membrane, Electrochim. Acta 159 (2015) 234–241.

[27] M. Ilgu, M. Nilsen-Hamilton, Aptamers in analytics, Analyst 141 (5) (2016) 1551–1568.

[28] S. Song, L. Wang, J. Li, C. Fan, J. Zhao, Aptamer-based biosensors, Trends Analyt. Chem. 27 (2) (2008) 108–117.

[29] X.-P. Zhao, J. Cao, X.-G. Nie, S.-S. Wang, C. Wang, X.-H. Xia, Label-free monitoring of the thrombin–aptamer recognition reaction using an array of nanochannels coupled with electrochemical detection, Electrochem. commun. 81 (2017) 5–9.

[30] K. Kant, J. Yu, C. Priest, J. G. Shapter, D. Losic, Impedance nanopore biosensor: influence of pore dimensions on biosensing performance, Analyst 139 (5) (2014) 1134–1140.

[31] I. Vlassiouk, T. R. Kozel, Z. S. Siwy, Biosensing with nanofluidic diodes, J. Am. Chem. Soc. 131 (23) (2009) 8211–8220.

[32] X. Wang, S. Smirnov, Label-free DNA sensor based on surface charge modulated ionic conductance, ACS Nano 3 (4) (2009) 1004–1010.

[33] K.-H. Paik, Y. Liu, V. Tabard-Cossa, M. J. Waugh, D. E. Huber, J. Provine, R. T. Howe, R. W. Dutton, R. W. Davis, Control of DNA capture by nanofluidic transistors, ACS Nano 6 (8) (2012) 6767–6775.

[34] S. Tseng, Y.-H. Tai, J.-P. Hsu, Ionic current in a ph-regulated nanochannel filled with multiple ionic species, Microfluid. Nanofluidics 17 (5) (2014) 933–941.

[35] H. Daiguji, P. Yang, A. Majumdar, Ion transport in nanofluidic channels, Nano Lett. 4 (1) (2004) 137–142.

[36] S. Movahed, D. Li, Electrokinetic transport through nanochannels, Electrophoresis 32 (11) (2011) 1259–1267.

[37] Y. Ma, J. Guo, L. Jia, Y. Xie, Entrance effects induced rectified ionic transport in a Nanopore/Channel, ACS Sens 3 (1) (2018) 167–173.

[38] R. D. Munje, S. Muthukumar, A. Panneer Selvam, S. Prasad, Flexible nanoporous tunable electrical double layer biosensors for sweat diagnostics, Sci. Rep. 5 (2015) 14586.

[39] P.-H. Lin, R.-H. Chen, C.-H. Lee, Y. Chang, C.-S. Chen, W.-Y. Chen, Studies of the binding mechanism between aptamers and thrombin by

circular dichroism, surface plasmon resonance and isothermal titration calorimetry, Colloids Surf. B Biointerfaces 88 (2) (2011) 552–558.

[40] D. Horn, D. Frondat, E. Ritzfl, The role of surface charge on the accelerating action of heparin on the antithrombin III-inhibited activity of &-thrombin, Plan. Perspect. 4598 (1985) 4603.

[41] G. Marson, M. Palumbo, C. Sissi, Folding versus charge: understanding selective target recognition by the thrombin aptamers, Curr. Pharm. Des. 18 (14) (2012) 2027–2035.

[42] I. Russo Krauss, A. Merlino, C. Giancola, A. Randazzo, L. Mazzarella, F. Sica, Thrombin–aptamer recognition: a revealed ambiguity, Nucleic Acids Res. 39 (17) (2011) 7858–7867.

[43] V. B. Tsvetkov, A. M. Varizhuk, G. E. Pozmogova, I. P. Smirnov, N. A. Kolganova, E. N. Timofeev, A universal base in a specific role: Tuning up a thrombin aptamer with 5-nitroindole, Sci. Rep. 5 (1) (2015) 16337.

[44] B. J. Kirby, Micro-and nanoscale fluid mechanics: transport in microfluidic devices, Cambridge university press, 2010.

[45] S. Kim, R. K. Anand, B. Ganapathysubramanian, Modeling electrochemical systems with weakly imposed dirichlet boundary conditions, arXiv preprint arXiv:2010.08778 (2020).

[46] J. S. Yoo, S. M. Park, An electrochemical impedance measurement technique employing fourier transform, Anal. Chem. 72 (9) (2000) 2035–2041.

[47] U. Bertocci, C. Gabrielli, F. Huet, M. Keddam, P. Rousseau, Noise resistance applied to corrosion measurements: II. experimental tests, Journal of The Electrochemical Society 144 (1) (1997) 37–43. doi:10.1149/1.1837362.
URL https://doi.org/10.1149/1.1837362

[48] C. Gabrielli, F. Huet, M. Keddam, Investigation of electrochemical processes by an electrochemical noise analysis. theoretical and experimental aspects in potentiostatic regime, Electrochimica Acta 31 (8) (1986) 1025–1039. doi:https://doi.org/10.1016/0013-4686(86)80018-4.
URL https://www.sciencedirect.com/science/article/pii/0013468686800184

[49] C. Gabrielli, M. Keddam, J. Lizee, Frequency analysis of electrochemical step responses complex and operational impedances, Journal of Electroanalytical Chemistry and Interfacial Electrochemistry 205 (1) (1986) 59–75. doi:https://doi.org/10.1016/0022-0728(86)90223-8.
URL https://www.sciencedirect.com/science/article/pii/0022072886902238

[50] P. Takmakov, I. Vlassiouk, S. Smirnov, Hydrothermally shrunk alumina nanopores and their application to DNA sensing, Analyst 131 (11) (2006) 1248–1253.

[51] J. C. Stachowiak, M. Yue, K. Castelino, A. Chakraborty, A. Majumdar, Chemomechanics of surface stresses induced by DNA hybridization, Langmuir 22 (1) (2006) 263–268.

[52] G. S. Manning, Limiting laws and counterion condensation in polyelectrolyte solutions i. colligative properties, J. Chem. Phys. 51 (3) (1969) 924–933.

[53] M. Szekeres, E. Tombácz, Surface charge characterization of metal oxides by potentiometric acid–base titration, revisited theory and experiment, Colloids Surf. A Physicochem. Eng. Asp. 414 (2012) 302–313.

[54] J. W. Ntalikwa, DETERMINATION OF SURFACE CHARGE DENSITY OF $\alpha\alpha$-ALUMINA BY ACID - BASE TITRATION, Bull. Chem. Soc. Ethiop. 21 (1) (2007) 117–128.

[55] C. Daniel, Y. Roupioz, D. Gasparutto, T. Livache, A. Buhot, Solution-phase vs surface-phase aptamer-protein affinity from a label-free kinetic biosensor, PLoS One 8 (9) (2013) e75419.

[56] X. Ma, A. Gosai, G. Balasubramanian, P. Shrotriya, Aptamer based electrostatic-stimuli responsive surfaces for on-demand binding/unbinding of a specific ligand, J. Mater. Chem. B Mater. Biol. Med. 5 (20) (2017) 3675–3685.

[57] T. Hianik, V. Ostatná, M. Sonlajtnerova, I. Grman, Influence of ionic strength, ph and aptamer configuration for binding affinity to thrombin, Bioelectrochemistry 70 (1) (2007) 127–133.

Table 1: Predicted and measured slopes of normalized nanochannel resistance changes at different quenching fractions at higher and lower electrolyte concentrations

Quenching ratio (q)	**Slopes**	
	Simulation	**Experiment**
	100 mM	
0 - 0.4	**0.028**	**0.24**
0.6 - 0.9	**-0.0024**	**-**
	1 mM	
0 - 0.4	**0.125**	**0.55**
0.6 - 0.9	**0.58**	**-**

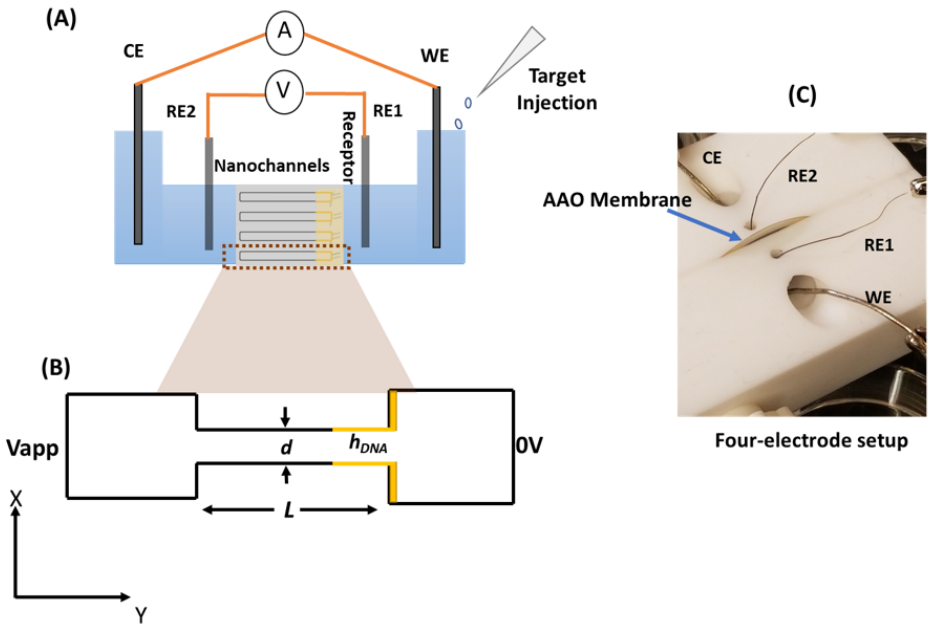

Figure 1: Schematic of the four-electrode setup (A) used for conducting the electrochemical impedance based sensing experiments- WE, CE, RE stand for Working, Counter and Reference Electrode respectively. An AC voltage of 5 mV is applied across the two REs and Current measured between WE and CE. Impedance is recorded over Frequency range of 0.1 Hz-100 kHz, Computational model (B) of Gold-coated asymmetric nanopore d = 20 nm, h_{DNA} = 0.25 μm and L = 1 μm and picture of the Teflon cell (C) used for experiments: Platinum electrodes are used as WE and CE, Ag/AgCl electrodes are used as REs

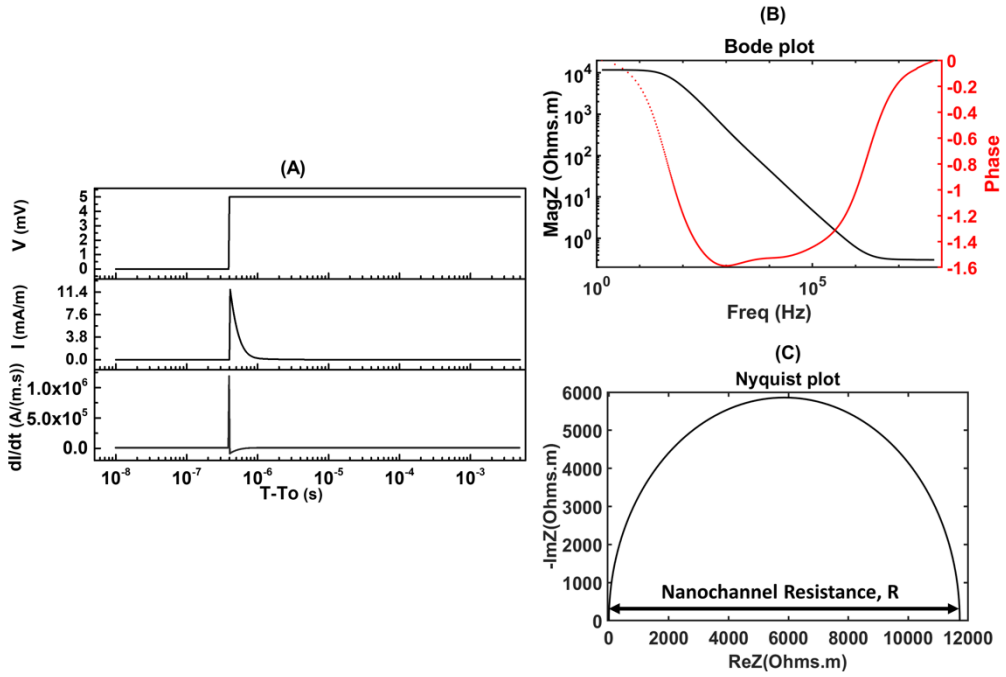

Figure 2: Current response, derivative of the current response (A) and the impedance response thus obtained by taking FFT (Bode (B) and Nyquist (C) plots) for an applied step voltage of 5 mV for σ_{DNA}= -5 mC/m^2 case

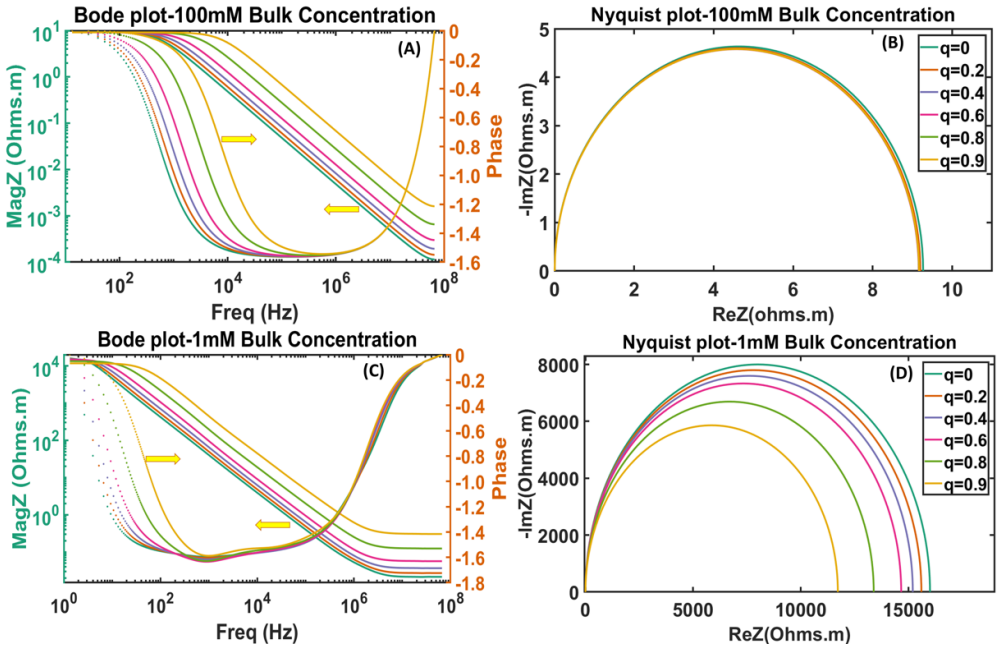

Figure 3: Bode and Nyquist plots with varying quenching ratios, $q = 0$ to 0.9, at 100 mM ((A) and (B))and 1 mM ((C) and (D) bulk electrolyte concentrations

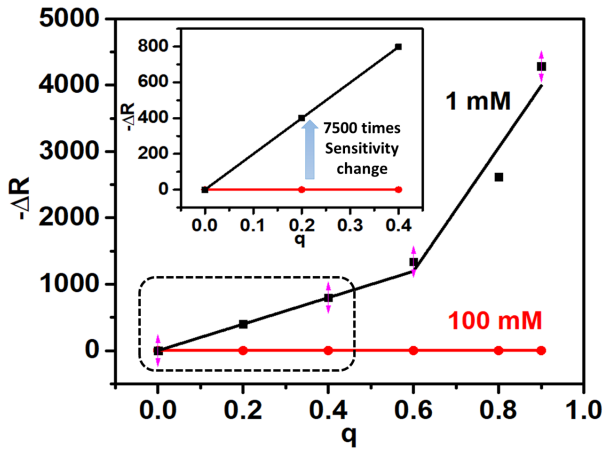

Figure 4: Nanochannel resistance changes, ΔR plotted as a function of quenching fractions, q at 100 mM and 1 mM bulk electrolyte concentrations. Inset shows the region focused on the q range of 0 to 0.4, which is the range of interest for thrombin and its aptamer

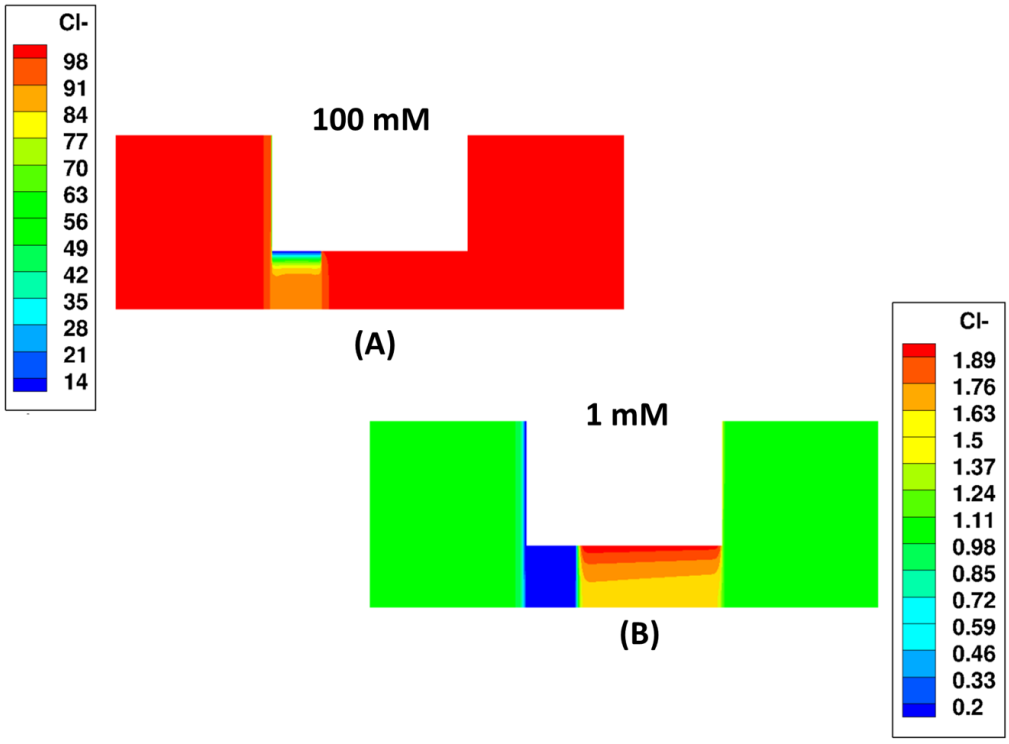

Figure 5: Contour plots of the concentration distribution of Cl^- ions in the nanochannel at bulk electrolyte concentrations of 100 mM and 1 mM for σ_{DNA} of -50 mC/m^2

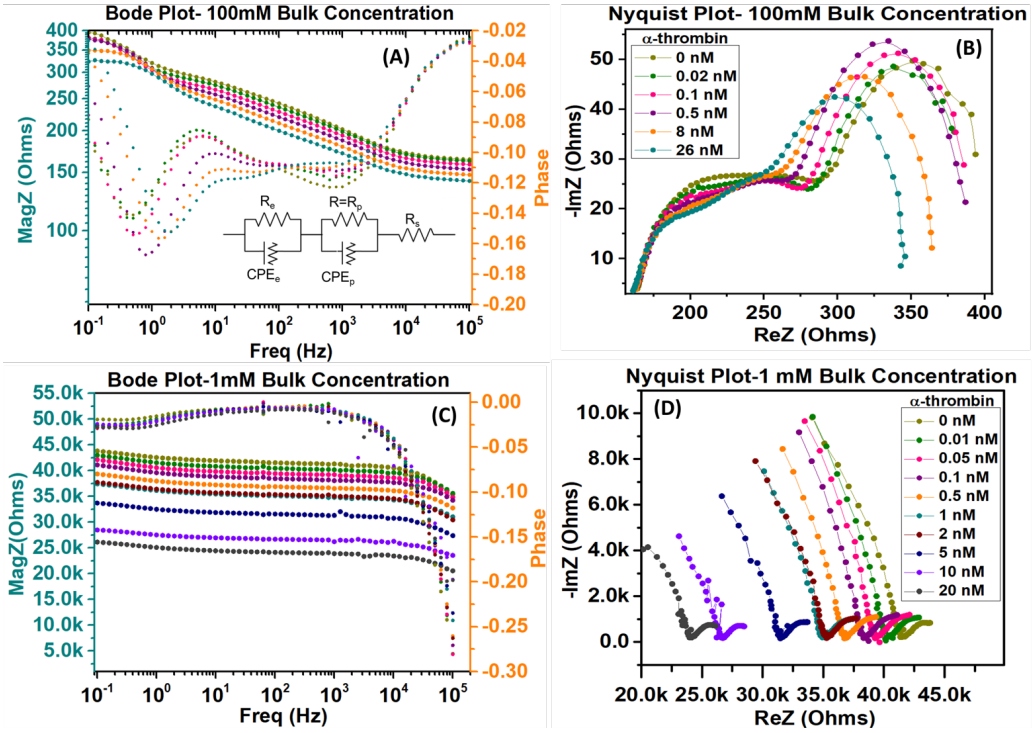

Figure 6: Experimentally measured impedance response- Bode and Nyquist plots for bulk electrolyte concentrations of 100 mM ((A) and (B)) and 1 mM ((C) and (D)) respectively. Inset in (A) shows circuit model used to analyze data

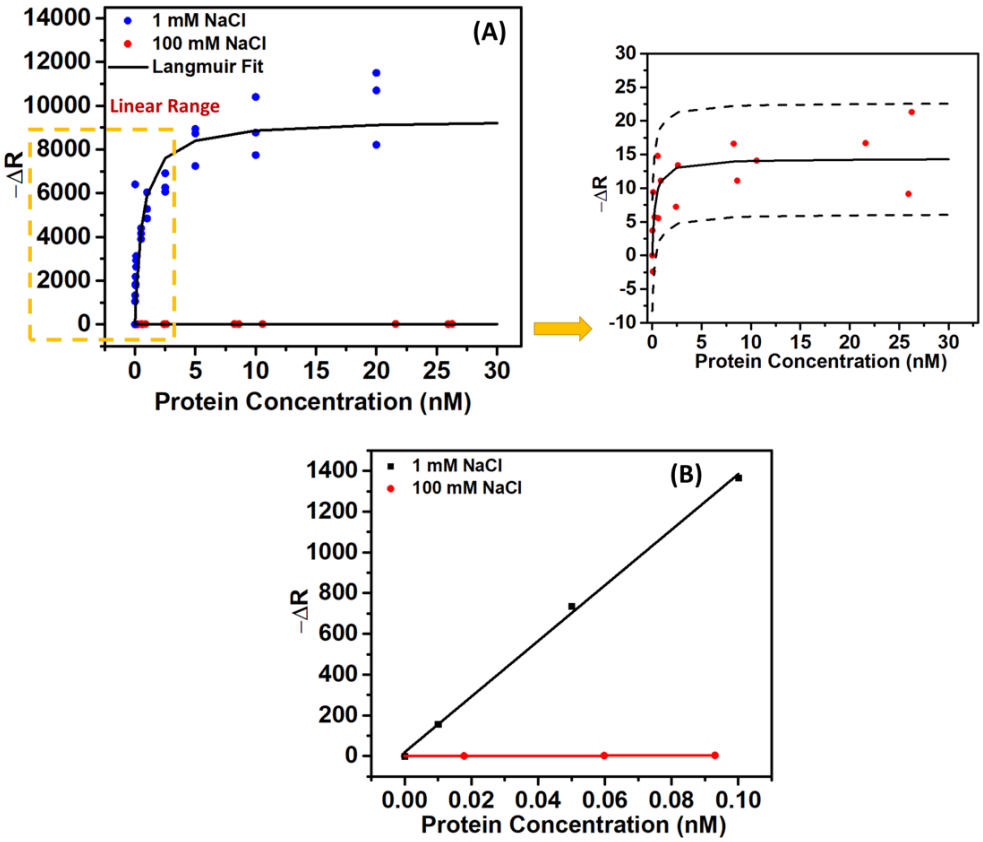

Figure 7: (A) Changes in nanochannel resistance (Sensor response) plotted as a function of protein concentration both at higher (100 mM) and lower (1 mM) electrolyte concentration. (B) shows comparison of sensitivities in the linear range of the sensor